Resistance and Threshold Switching Voltage Drift Behavior in Phase-Change Memory and Their Temperature Dependence at Microsecond Time Scales Studied Using a Micro-Thermal Stage

SangBum Kim, Byoungil Lee, Mehdi Asheghi, Fred Hurkx, John P. Reifenberg, Kenneth E. Goodson, and H.-S. Philip Wong

***Abstract*—We study the drift behavior of RESET resistance R_{RESET} and threshold switching voltage V_{th} in phase-change memory (PCM) and their temperature dependence. To extend the temperature-dependent measurement to microsecond time scales, we integrate an innovative micro-thermal stage (MTS) on the PCM cell. The MTS changes the temperature of the programmed region of the PCM cell within a few microseconds by placing the Pt heater in close proximity of the programmed region. First, we experimentally verify the existing phenomenological R_{RESET} and V_{th} drift model for constant annealing temperature at various temperatures between 25 °C and 185 °C down to 100 μs and show that the measured temperature dependence of the drift coefficient agrees well with what is expected from the existing drift models. Based on the existing drift model for a constant annealing temperature, we derive the analytical expression for the R_{RESET} drift for time-varying annealing temperature and experimentally verify the analytical expression. The derived analytical expression is important to understand the impact of thermal disturbance on PCM reliability such as variations in R_{RESET} and V_{th}.**

***Index Terms*—Nonvolatile memory, phase-change memory (PCM), resistance drift, threshold switching.**

I. Introduction

PHASE-CHANGE MEMORY (PCM) is one of the maturest candidates for a next-generation nonvolatile memory [1]. PCM provides a new set of features in the memory application field including nonvolatility, good endurance, bit alterability, and fast read and write [2]. PCM stores data by changing the structural phase of a chalcogenide material. The two memory states correspond to a crystalline phase with low resistivity (the SET state) and an amorphous phase with high resistivity (the RESET state). The phase change in the PCM cell is thermally induced by electrical Joule heating. The electrical resistance of the written cell is read to determine the stored phase.

The scalability and reliability of PCM are key issues to be solved in order to broaden its application among memory devices. It requires understanding of the basic physical properties of the phase-change material related to the PCM operation, such as the threshold switching phenomenon [3]–[5], the drift behavior [6]–[10], the recovery behavior [11], and the material property scaling [12]. Among them, the drift behavior is the key factor that determines multibit capability and reliability. The drift behavior is described as the continuous drift of the RESET state after the material has been melted and quenched. As a result, the electrical characteristics of the RESET state including the RESET resistance and the threshold switching voltage drift after the cell is programmed in the RESET state. The physics involved in the drift behavior is still debated. In the past years, several theoretical models have been proposed based on trap decay, which reduces conductivity in the trap-assisted conduction model [7]–[9], generation of the donor/acceptor defect pairs, which reduces conductivity by repositioning the Fermi level [6], [13], and mechanical stress release, which widens the energy gap between the Fermi level and the mobility edge [10]. There have been experimental studies on the temperature dependence of the drift behavior using the conventional hot stage or plate to compare with what various models predict [8]–[10], [14], [15]. Due to the large thermal time constant of the conventional hot stage or plate, temperature-dependent measurements were conducted at time scales of a few seconds or more, and the results were extrapolated over five to six orders of magnitude down to a few microseconds. Therefore, the experimental demonstration of the validity of the extrapolation is still important to understand the physics behind the drift phenomenon.

The temperature dependence of the drift behavior in the microsecond time scale is also important to understand the effect of thermal disturbance on PCM operation [16]. Thermal disturbance refers to a situation in which the heat diffusion from the programmed region during RESET programming causes

Manuscript received May 13, 2010; revised November 10, 2010; accepted November 12, 2010. Date of publication January 10, 2011; date of current version February 24, 2011. This work was supported in part by NXP, by the National Science Foundation under Grant CBET-0853350, by the Global Research Collaboration of the Semiconductor Research Corporation under Contract 2009-VJ-1996, by the member companies of the Stanford Non-Volatile Memory Technology Research Initiative (NMTRI), and by the Materials, Structures and Devices Focus Center, which is one of six research centers funded under the Focus Center Research Program, a Semiconductor Research Corporation entity. The work of S. Kim is supported by Samsung Fellowship. The review of this paper was arranged by Editor G. Jeong.

S. Kim is with the IBM T. J. Watson Research Center, Yorktown Heights, NY 10598 USA (e-mail: SangBum.Kim@us.ibm.com).

B. Lee, M. Asheghi, K. E. Goodson, and H.-S. P. Wong are with Stanford University, Stanford, CA 94305 USA.

F. Hurkx is with NXP-TSMC Research Center, 3001 Leuven, Belgium.

J. P. Reifenberg is with Intel Corporation, Santa Clara, CA 95054 USA.

Color versions of one or more of the figures in this paper are available online at http://ieeexplore.ieee.org.

Digital Object Identifier 10.1109/TED.2010.2095502

0018-9383/$26.00 © 2011 IEEE

temperature rise in the adjacent cells. Temperature rise in the adjacent cells can unintentionally crystallize the cell, resulting in retention failure when the thermal disturbance effect is accumulated over time [17], [18]. In addition, the temperature rise can expedite the drift behavior of the cell resulting in larger RESET resistance R_{RESET} and threshold switching voltage V_{th} variations [16]. The effect of the thermal disturbance in a scaled device can become even larger as cell distances decrease due to aggressive scaling that scales the cell distances more aggressively than the vertical dimension [18]. To our best knowledge, an analytical prediction for the impact of the short temperature rise (e.g., thermal disturbance) on the drift has not been provided yet.

In this paper, we extend the temperature-dependent drift measurement down to a microsecond time scale, which is the relevant time scale for PCM operation. We measure both R_{RESET} and V_{th} drift behavior, which represent the drift of the RESET state. With these new measurement results, we verify the existing phenomenological drift model for constant annealing temperature down to 100 μs, without extrapolation. The key enabler for these new measurements is the micro-thermal stage (MTS). The MTS consists of the lateral PCM cell and the Pt heater for changing the temperature of the PCM cell in microseconds. Finally, we present the analytical expression for the drift with time-varying annealing temperature, which can predict the impact of thermal disturbance on the drift. The analytical prediction agrees well with the measurement results using the MTS.

II. Drift Model and Its Temperature Dependence

The drift behavior of PCM is described as the continuous drift of the RESET state after the material has been melted and quenched [6]–[10]. As the RESET state drifts, the measurable quantities such as R_{RESET} and V_{th} that represent the RESET state also drift. Regardless of differences in the proposed mechanisms for the drift behavior, experimental data on R_{RESET} and V_{th} drifts for constant annealing temperature were phenomenologically described by the following equations that were either derived [10] or replicated by a calculation [6]–[8] in each model:

$$R_{\mathrm{RESET}}(t) = R_0 \left(\frac{t}{t_0}\right)^{\nu} \tag{1}$$

$$V_{\mathrm{th}}(t) = V_{\mathrm{th0}} + \log\left(\frac{t}{t_0}\right)^{\alpha} \tag{2}$$

where t, ν, and α are the time after RESET programming, the R_{RESET} drift coefficient, and the V_{th} drift coefficient, respectively. R_0, and V_{th0} are the prefactors for resistance and voltage, respectively, and t_0 is the time constant.

To theoretically model the temperature dependence of the drift behavior, we base our analysis on the trap decay model [7]–[9], which has been expressed in analytical forms with detailed description of most physics involved. The energy barrier for trap decay in the proposed model results in strong temperature dependence [14]. To theoretically estimate the temperature dependence of the drift coefficients ν and α, we assume that R_{RESET} and V_{th} are determined by the trap density N_T. According to the trap decay model, where traps are characterized by a distribution of trap energy and an initial trap density, the total trap density $N_T(t)$ in the case of constant annealing temperature is given by the following equation [7], [9], [14]:

$$N_T(t) = N_{T0}\left(\frac{t}{t_0}\right)^{-\frac{kT_A}{\sigma}} \quad (\text{for } t \gg t_0) \tag{3}$$

where N_{T0}, k, T_A, and σ are the initial total trap density, the Boltzmann constant, the annealing temperature, and the energy decay constant, respectively. The drift coefficient for R_{RESET} can be related to N_T by the following equation, and it shows that it is proportional to annealing temperature T_A:

$$\begin{aligned}\nu &= \frac{d\ln R_{\mathrm{RESET}}(t)}{d\ln t} = \frac{d\ln R_{\mathrm{RESET}}(t)}{d\ln N_T(t)}\frac{d\ln N_T(t)}{d\ln t} \\ &= \frac{d\ln R_{\mathrm{RESET}}(t)}{d\ln N_T(t)}\cdot\left(-\frac{kT_A}{\sigma}\right) \propto T_A. \end{aligned} \tag{4}$$

The $d\ln R_{\mathrm{RESET}}(t)/d\ln N_T(t)$ term also has the temperature dependence, but it depends on the reading temperature T_R, not T_A. The same derivation can be applied to the drift coefficient for V_{th}, and it can be shown that it is also proportional to T_A. When the Meyer–Neldel effect is considered, the temperature dependence of the R_{RESET} drift coefficient is expressed in a slightly different form that is proportional to $T_A/(1 - T_A/T_{\mathrm{MN}})$ [15], where T_{MN} is the compensation temperature. However, the overall tendency generally agrees well considering that T_{MN} is relatively high [15] compared with the annealing temperature in consideration.

To experimentally measure the temperature dependence of the drift coefficients, the programming and reading temperatures T_P and T_R should be constant while changing the annealing temperature T_A because nonconstant T_P and T_R complicates the interpretation of measurement data by adding secondary effects. For example, T_P determines the initial RESET state such as the amorphous region size and the initial trap density. In addition, the same number of traps may be represented by different R_{RESET}, V_{th}, and ν at different T_R [5], [6], [19], [20]. An experimental procedure that separates the impact of T_A on the drift from the impact of T_R on the measurement results even when T_A and T_R are identical has been proposed [20]. However, it is still not applicable to measurements in a microsecond time scale because it is still required to independently control T_P from T_A or T_R. Therefore, in the following experiment as well as modeling, we maintained T_P and T_R at room temperature while changing only T_A to distinguish and study the effect of temperature on the drift. To extend these temperature-dependent measurements to microseconds that are the relevant time scale for PCM operation, a faster heater is required, which has a thermal time constant in the microsecond time scale because T_A is not necessarily the same as T_P and T_R. We implement such a fast heater with the MTS.

III. Micro-Thermal Stage

The thermal time constant or speed of the temperature controller is determined by the total thermal mass of the system.

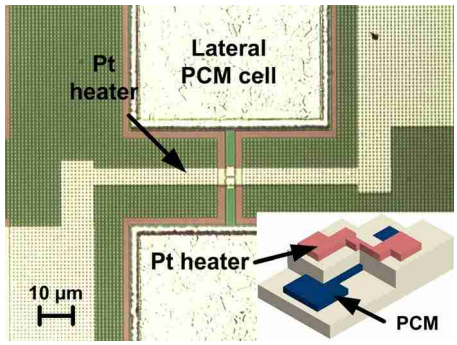

Fig. 1. Microscope image of an MTS. Pt heater is integrated on top of the lateral PCM cell. (Three-dimensional figure inset) The Pt heater overlapped region over narrow phase-change-material programmed region.

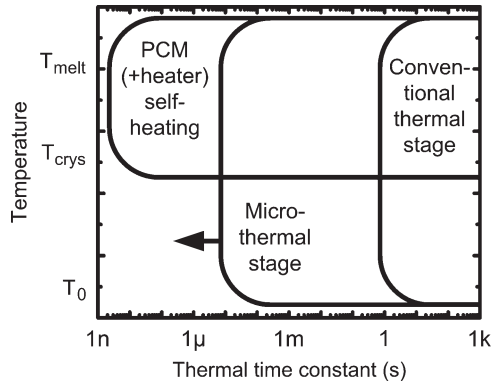

Fig. 2. MTS extends temperature control down to a microsecond time scale or below that is not accessible by conventional thermal stages with large thermal time constants. Precise temperature control below crystallization temperature $T_{\rm crys}$ is enabled by the MTS in contrast to phase-change material self-Joule heating, which suffers from sudden increase in temperature caused by the threshold switching. Due to its extended temporal resolution, programming T_P, annealing T_A, and reading temperatures T_R can be independently controlled.

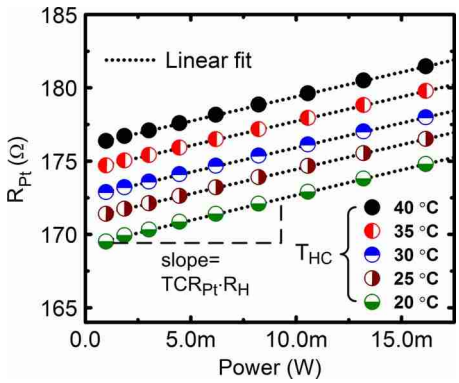

Fig. 3. Resistance of the Pt heater linearly increases as temperature increases. The temperature of the Pt heater is determined by the electrical power provided to the Pt heater and hot-chuck temperature $T_{\rm HC}$. By fitting the experimental results to (5), the amount of temperature rise can be determined from the electrical power, i.e., P. From the resistance difference for various $T_{\rm HC}$ at constant P, $\rm TCR_{Pt}$ is extracted first. Thermal resistance R_H can be extracted from the slope gradient from linear fitting, which is the product of $\rm TCP_{Pt}$ and R_H. The temperature rise for the given P is the product of R_H and P.

Therefore, by positioning the heat source near the target region, the thermal mass and the thermal time constant can be reduced. The MTS implements this design concept. Fig. 1 shows the lateral PCM cell integrated with the MTS. First, the lateral PCM cell is fabricated, as reported in [21]. A 20-nm-thick doped SbTe alloy is deposited by sputtering and patterned by reactive ion etching in a line cell. After pattering, the PCM cells were passivated using a $\sim$1-μm-thick combination of silicon oxide and silicon nitride. On top of the passivation layer, the 80-nm-thick Pt bridge as a heater is patterned. The inset figure in Fig. 1 shows the 3-D structure of the MTS. By generating Joule heat in the Pt heater, the temperature of the programmed region of the PCM cell is controlled. The Pt heater is only $\sim$1 μm away from the programmed region, resulting in 1.53 and 1.27 μs of thermal time constant for the programmed region and Pt heater, respectively. Additional thermal time constant of 0.26 μs can be attributed to the delay time for generated heat to travel from the Pt heater to the programmed region. The width of the Pt heater (5 μm) is much wider than the size of the programmed region (200 nm by 400 nm) to ensure uniform temperature rise in the programmed region. The power delivered to the Pt heater can be precisely controlled by controlling the voltage amplitude to the Pt heater, resulting in accurate control of the amount of temperature rise for a wide range of temperatures. Note that if the temperature is controlled by the self-Joule heating of the phase-change material, the large conductivity difference before and after threshold switching makes it difficult to control the amount of temperature rise, particularly for a temperature range below the crystallization temperature. In addition, the self-Joule heating of the phase-change material may accompany unintentional electronic effects on the drift such as reinitiation of the drift after threshold switching, even without melt quenching [6], which makes it difficult to distinguish temperature-dependent effects. The applicable range of the thermal time constant and the temperature range of the MTS is compared with conventional methods in Fig. 2.

The temperature of the MTS is calibrated by the temperature dependence of the resistance of the Pt heater. Most of the heat generated in the Pt heater propagates downward toward the Si substrate because the thermal resistance between the Pt heater and the Si substrate (i.e., heat sink) is low enough to efficiently remove most of the heat. Downward heat conduction can be treated as 1-D conduction because the width of the Pt heater is much larger than the thickness of underlying layers. Therefore, the temperature is almost constant along the Pt heater during Joule heating in the steady state. Since the resistivity of most metals linearly increases as the temperature increases [22], the temperature rise from Joule heating can be measured from the resistivity change of the heater. In steady state, the resistivity of the Pt heater $\rho_{\rm Pt}$ on the temperature-controlled hot chuck is given by

$$\boldsymbol{\rho_{Pt} = \rho_0 + TCR_{Pt} \cdot (T_{HC} + P \cdot R_H)} \tag{5}$$

where $\rm TCR_{Pt}$, $T_{\rm HC}$, P, R_H are the temperature coefficient of the resistance of Pt, the temperature of hot chuck on which the sample is placed, the power delivered to the Pt heater, and the thermal resistance between the Pt heater and the chuck, respectively. After calibrating the resistance of the Pt heater with the heater power and the chuck temperature $T_{\rm HC}$, as in Fig. 3, the temperature rise of the Pt heater can be determined once the power provided to the Pt heater is known.

In steady state, the ratio of the temperature rise of the programmed region in the PCM cell to the temperature rise of the Pt heater is constant and determined by the ratio of their thermal resistances to ambient temperature. The temperature of the programmed region of the PCM cell can be calibrated using the temperature dependence of the RESET resistance of the PCM cell because the resistivity of the amorphous region is highly dependent on the temperature [5], [6], [19]. By comparing the resistivity of the amorphous region on the MTS with those at various temperatures of hot chuck, the temperature rise of the programmed region can be directly determined from the electrical power delivered to the Pt heater.

IV. Experimental Results and Discussion

To study the dependence of the drift on the annealing temperature, we apply separate electrical pulses to the PCM cell and the Pt heater. The electrical pulse to the PCM cell programs the cell and measures cell characteristics such as R_{RESET} and V_{th}. The electrical pulse to the Pt heater controls the temperature of the programmed region of the PCM cell. The timing of the electrical pulses is precisely controlled using triggering signals and internal timers of pulse generators.

A. RESET Resistance Drift for Constant Annealing Temperature

We experimentally verify the existing phenomenological R_{RESET} drift model for constant annealing temperature in microsecond time scale. To measure the temperature dependence of the R_{RESET} drift coefficient, we vary the annealing temperature T_A between 25 °C (no annealing) and 185 °C. The PCM cell is RESET-programmed with RESET/SET resistance ratio of ∼1000 and read at 25 °C, without any heating from the Pt heater (i.e., $T_P = T_R = 25$ °C). The annealing pulse started at 10 μs after RESET programming. The 10-μs time margin guarantees that the programmed region quenches to 25 °C after RESET programming to achieve identical initial RESET states. The reading pulse is 20-μs long, and the annealing pulse is turned off 40 μs before reading and restarts 40 μs after the reading. The 40-μs time margins guarantee that the programmed region constantly stays at 25 °C throughout reading. The current-to-voltage amplifier makes short reading time of 20 μs sufficient to read the R_{RESET} with accuracy of less than 2%. The read bias voltage is 0.4 V. The R_{RESET} is read at 100 μs; 1, 10, 100 ms; and 1 s plus time-margins after RESET programming. Time margins contribute to measurement errors because the programmed region is not annealed during the time margins. These errors from time margins can be compensated in the later calculation for the drift coefficient. The shape and timing of the electrical pulse and resultant temperature are shown in Fig. 4.

Fig. 5(a) shows the R_{RESET} drift over time for various T_A. Each data point is from ∼100 measurements such that random variations are averaged out. The R_{RESET} drift behavior in Fig. 5(a) follows the power law, as described in (1). Therefore, the R_{RESET} drift coefficient in (1) can be extracted for various T_A. Fig. 5(b) shows the R_{RESET} drift coefficient calculated from the data in Fig. 5(a) for various T_A. At low temperature, the drift coefficient linearly increases, as shown by (4). At high temperature, the drift coefficient slowly increases and even decreases possibly due to simultaneous crystallization at high temperatures [15] or drift saturation [10]. By finding the intersection points between extrapolated lines at various T_A from the data in Fig. 5(a), t_0 and R_0 are found to be between 10 ns and 1 ps and between 400 and 600 kΩ, respectively.

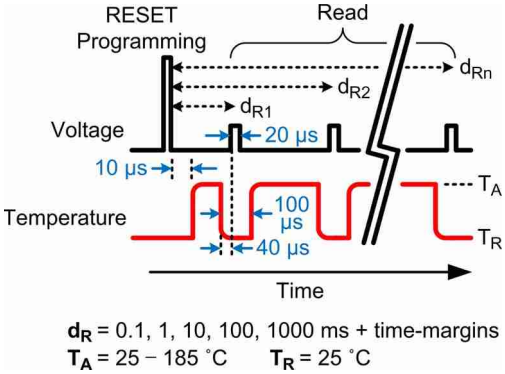

Fig. 4. Electrical pulse and temperature profile for R_{RESET} drift measurement. The measurement results are shown in Fig. 5. The cells are programmed and read at room temperature (25 °C). The cell resistances are read by small read voltage pulses at multiple delay times for reading, i.e., d_R. The cells are annealed at various annealing temperature T_A between 25 °C and 185 °C by the Pt heater.

B. RESET Resistance Drift for Time-Varying Annealing Temperature

In a practical scenario for a PCM cell in operation, the annealing temperature may not be constant because cells can be thermally disturbed by the RESET programming of the neighboring cells [16]–[18]. Then, how can we estimate the actual R_{RESET} trace for those thermally disturbed cells? The simple form in (1) cannot be directly applied to this case because (1) assumes that annealing temperature stays constant after RESET programming. If the annealing temperature is continuously changing as $T_A(t)$, the R_{RESET} drift speed is dependent on the present trap density, trap energy distribution, and annealing temperature T_A. The present trap density and trap energy distribution can be represented by $R_{\mathrm{RESET}}(T_R, t)$, which is R_{RESET} measured at reading temperature T_R and time t after RESET programming. We assume that the same $R_{\mathrm{RESET}}(T_R, t)$ corresponds to the same RESET state characterized by the same number of traps with identical trap energy distribution. To derive a partial differential equation for $R_{\mathrm{RESET}}(T_R, t)$ for time-varying annealing temperature $T_A(t)$, we express $R_{\mathrm{RESET}}(T_R, t + \Delta t)$ in terms of $R_{\mathrm{RESET}}(T_R, t)$ and $T_A(t + \Delta t)$ for infinitesimal time step Δt, as in the following equation:

$$\begin{aligned} &R_{\mathrm{RESET}}(T_R, t + \Delta t) \\ &\quad = R_0 \left\{ \frac{\Delta t + t_{\mathrm{eff}}}{t_0} \right\}^{\nu(T_A(t+\Delta t))} \\ &\quad = R_0 \left\{ \frac{\Delta t}{t_0} + \left[\frac{R_{\mathrm{RESET}}(T_R, t)}{R_0} \right]^{\frac{1}{\nu(T_A(t+\Delta t))}} \right\}^{\nu(T_A(t+\Delta t))} \end{aligned} \tag{6}$$

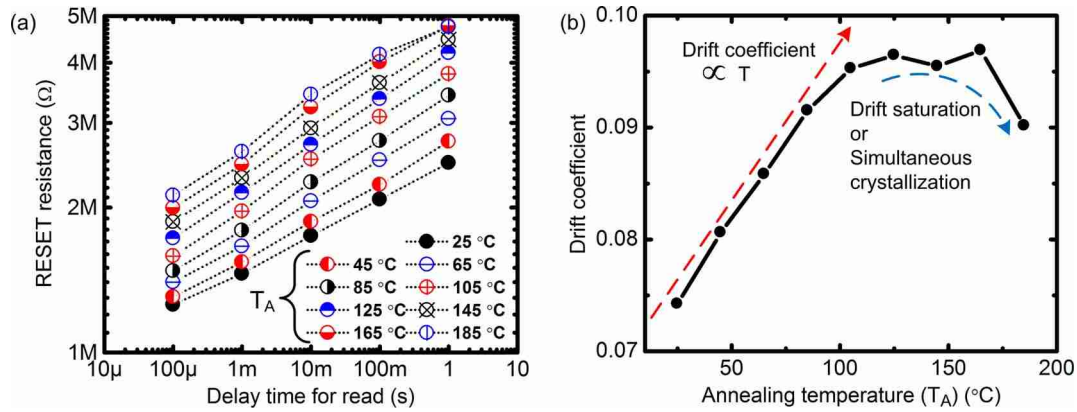

Fig. 5. (a) RESET resistance as a function of time after RESET programming for various annealing temperatures T_A. (b) R_{RESET} drift coefficient calculated from the data in (a). The cells are programmed and read at room temperature (25 °C). The R_{RESET} drift coefficient linearly increases as T_A increases below ~100 °C. Possibly due to drift saturation or simultaneous crystallization process, the drift coefficient decreases at high temperatures. The details of the measurement pulse are shown in Fig. 4.

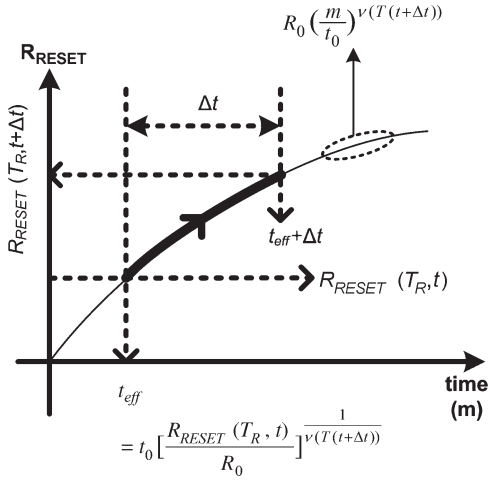

Fig. 6. Schematic for derivation of (6), which derives $R_{\mathrm{RESET}}(T_R, t + \Delta t)$ in terms of $R_{\mathrm{RESET}}(T_R, t)$, Δt, and $T_A(t + \Delta t)$. $T_A(t + \Delta t)$ is the annealing temperature between t and $t + \Delta t$. The curve on the figure represents the RESET resistance drift trace that would have been followed if the annealing temperature were constant at $T_A(t + \Delta t)$ since the RESET programming. First, t_{eff} is calculated from $R_{\mathrm{RESET}}(T_R, t)$. t_{eff} is the time that it would have taken for RESET resistance to drift to $R_{\mathrm{RESET}}(T_R, t)$ if the annealing temperature had been constant at $T_A(t + \Delta t)$ since the RESET programming. The RESET resistance drifts for a time period of Δt, following the curve from t_{eff} to $t_{\mathrm{eff}} + \Delta t$. $R_{\mathrm{RESET}}(T_R, t + \Delta t)$ is determined as the RESET resistance that corresponds to $t_{\mathrm{eff}} + \Delta t$ on the time axis.

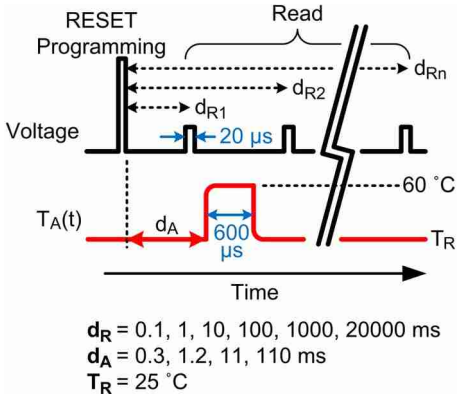

Fig. 7. Electrical pulse and temperature profile for R_{RESET} drift measurement. The measurement results are shown in Fig. 8. The cells are programmed and read at room temperature (25 °C). d_A and d_R are delay time for annealing and reading, respectively. The heat pulse is 600-μs long and 60 °C high.

where t_{eff} is the time that it would have taken for RESET resistance to drift to $R_{\mathrm{RESET}}(T_R, t)$ if the annealing temperature had been constant at $T_A(t + \Delta t)$ from the time when it was RESET programmed (as in the drift model for constant annealing temperature). Between t and $t + \Delta t$, the RESET state drifts at the annealing temperature of $T_A(t + \Delta t)$. The derivation of (6) is graphically represented in Fig. 6. Equation (6) leads to the following partial differential equation:

$$\frac{d\left(\ln R_{\mathrm{RESET}}(T_R,t)\right)}{dt} = \frac{\nu\left(T_A(t)\right)}{t_0}\left(\frac{R_0}{R_{\mathrm{RESET}}(T_R,t)}\right)^{\frac{1}{\nu(T_A(t))}}. \tag{7}$$

From (7), $R_{\mathrm{RESET}}(T_R, t)$ can be numerically determined for the given $T_A(t)$ once we know $\nu(T_A)$, t_0, and R_0 at T_R. To determine the validity of (7), we compare the measurement results with the prediction. The prediction is numerically calculated from (7) based on $\nu(T_A)$, R_0, and t_0 obtained from Fig. 5. $T_A(t)$ shown in Fig. 7 is implemented using the Pt heater on the MTS. We vary d_A and measure R_{RESET} at various d_R, where d_A and d_R are delay times for annealing and reading, respectively. The temperature and duration of the annealing pulse are 60 °C and 600 μs, respectively. The R_{RESET} is read at 100 μs; 1, 10, and 100 ms; and 1 and 20 s after RESET programming. The programming and reading is at 25 °C, without any heating from the Pt heater. d_A is varied at 300 μs and 1.2, 11, and 110 ms.

Fig. 8(a) shows the measured R_{RESET} drift over time for various d_A. Each data point is from ~100 measurements such that random variations are averaged out. R_{RESET} at 100 μs are the same for various d_A verifying that the initial RESET states are the same. As shown in Fig. 8(b), where the percentage change from $R_{\mathrm{RESET}}(t)$ without any annealing is plotted, annealing at d_A of 300 μs, which is the shortest in this experiment, shows the largest percentage increase. This can be deduced from the resistance drift model in (7), which shows larger percentage

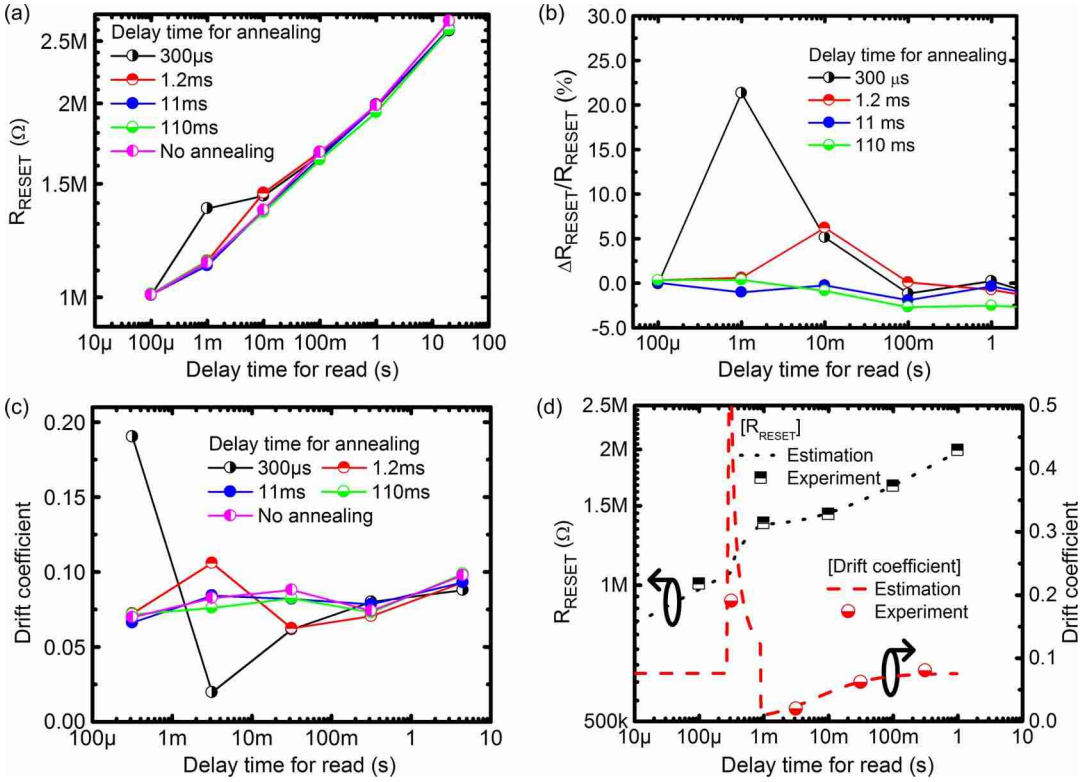

Fig. 8. (a) $R_{\mathrm{RESET}}(t)$ for various delay time for annealing, i.e., d_A. (b) The percentage difference of $R_{\mathrm{RESET}}(t)$ with respect to $R_{\mathrm{RESET}}(t)$ without any annealing. Shorter d_A results in larger percentage difference during annealing. (c) R_{RESET} drift coefficient calculated from (a). The R_{RESET} drift coefficient dramatically changes during and right after annealing for small d_A. (d) The estimation based on (7) agrees well with the measurement results. The case when d_A is 300 μs is shown here. The cells are programmed and read at room temperature (25 °C). The details of the measurement pulse are shown in Fig. 7.

change $(d(\ln R_{\mathrm{RESET}}(T_R,t))/dt)$ for smaller $R_{\mathrm{RESET}}(T_R,t)$. Therefore, if the temperature and the duration of the annealing are the same, the shortest d_A results in the largest percentage increase. This suggests that a single thermal disturbance has the largest immediate impact on R_{RESET} when it has the shortest time delay after RESET programming.

Fig. 8(c) shows the averaged R_{RESET} drift coefficient $(\Delta \ln(R_{\mathrm{RESET}}(T_R,t))/\Delta \ln(t))$ extracted from the same set of data in Fig. 8(a). When d_A is short, the extracted averaged drift coefficient for time period that has an annealing pulse in it, is much larger than the drift coefficient at 60 °C in Fig. 5(b). For example, the averaged ν between 100 μs and 1 ms for d_A of 300 μs is close to 0.2, whereas $\nu(60\ ^\circ\mathrm{C})$ is only $\sim$0.085 in Fig. 5(b). This rather nonintuitive result is due to the fact that $\nu(T_A)$ is the R_{RESET} drift coefficient when the cell is continuously annealed at T_A, which is not the case in this measurement. In this measurement, the cell was not annealed at the beginning, which leaves intact traps that would have otherwise decayed if the cell is continuously annealed at T_A. Therefore, when the annealing started at d_A, these remaining traps decay very rapidly, resulting in a drift coefficient higher than $\nu(T_A)$. The same mechanism is responsible for the reduced drift coefficient after the annealing stops. Some traps at low trap energy had already decayed at the elevated annealing temperature T_A, and this leaves less traps to decay later on at the room temperature. Fig. 8(c) clearly shows this effect where the drift coefficient is reduced below $\nu(25\ ^\circ\mathrm{C})$ after the annealing. This effect of early expedited or impeded decay can be better understood by simply inserting a time shift term $\Delta t_{\mathrm{shift}}$ in the drift equation, i.e., (1). $\Delta t_{\mathrm{shift}}$ enables us to analyze the drift behavior with the time-varying annealing temperature using

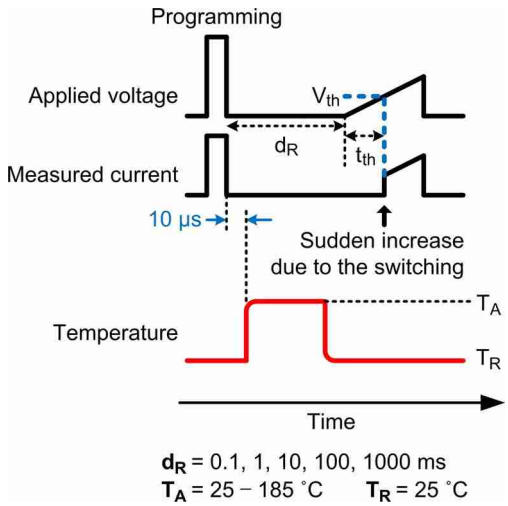

Fig. 9. Electrical pulse and temperature profile for the V_{th} drift measurement. The measurement results are shown in Fig. 10. The cells are programmed and read at room temperature (25 °C). The cells are annealed by the Pt heater at annealing temperature T_A between 25 °C and 185 °C. The reading pulse for V_{th} is applied after the delay time for reading, i.e., d_R, which varies between 0.1 μs and 1 s. The reading pulse for V_{th} is a single triangular pulse that causes sudden increase in current when the amplitude reaches V_{th}. By measuring t_{th}, which is the time it takes to threshold switch, V_{th} is determined as the product of t_{th} and the voltage ramp rate.

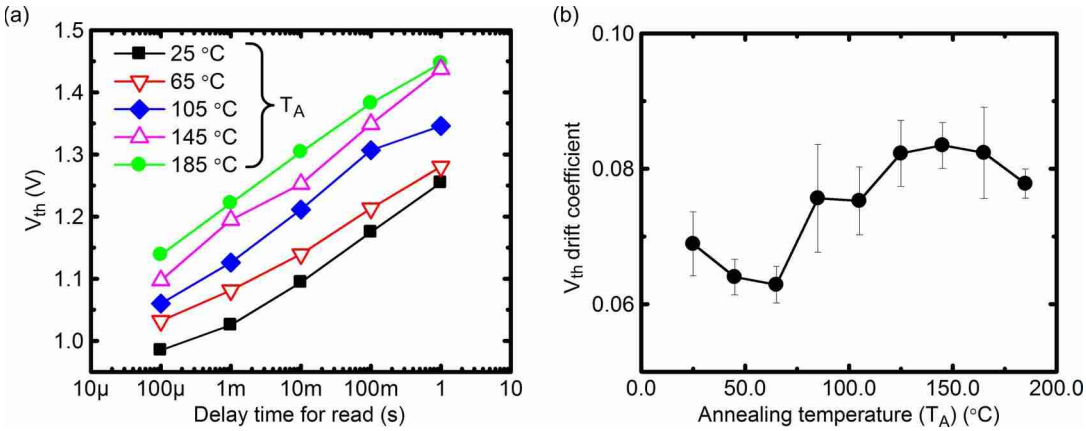

Fig. 10. (a) $V_{\rm th}(t)$ for various annealing temperatures T_A. (b) The $V_{\rm th}$ drift coefficient as a function of T_A calculated from (a). It shows the tendency to increase as T_A increases and agrees with the temperature dependence of the $R_{\rm RESET}$ drift coefficient. The cells are programmed and read at room temperature (25 °C). The measurement pulse details are shown in Fig. 9.

a simpler form of the drift equation for constant annealing temperature, as shown by the following equation:

$$R_{\rm RESET}(T_R,t)=R_0\left(\frac{t+\Delta t_{\rm shift}}{t_0}\right)^{\nu(T_A)}. \tag{8}$$

If the annealing temperature has been previously deviated from T_A, its overall effect can be accounted by $\Delta t_{\rm shift}$. $\Delta t_{\rm shift}$ can be found so that $R_{\rm RESET}(T_R,t)$ calculated from (8) is identical to that calculated from (7). Equation (8) leads to the effective drift coefficient $\nu_{\rm eff}$ to be as follows:

$$\begin{aligned}\nu_{\rm eff}&=\frac{d\ln R_{\rm RESET}(T_R,t)}{d\ln t}=\frac{d\ln R_{\rm RESET}(T_R,t)}{dt}\frac{dt}{d\ln t}\\&=\nu(T_A)\frac{t}{t+\Delta t_{\rm shift}}\end{aligned} \tag{9}$$

where $\nu(T_A)$ is the $R_{\rm RESET}$ drift coefficient for the constant annealing temperature of T_A. For zero $\Delta t_{\rm shift}$, i.e., the cell is continuously annealed at T_A, $\nu_{\rm eff}$ is the same as $\nu(T_A)$. For positive $\Delta t_{\rm shift}$, i.e., the cell has less traps because the traps at low trap energy have already decayed due to preannealing temperature that is higher than T_A, $\nu_{\rm eff}$ is smaller than $\nu(T_A)$. For negative $\Delta t_{\rm shift}$, i.e., the cell has more traps because the trap decay has been impeded by preannealing temperature that is lower than T_A, $\nu_{\rm eff}$ is larger than $\nu(T_A)$. As shown in Fig. 8(c), $\Delta t_{\rm shift}$ becomes negligible as t increases, and $\nu_{\rm eff}$ converges to $\nu(T_A)$. Fig. 8(d) shows that the prediction from (7) agrees well with the measurement results for both $R_{\rm RESET}$ and its drift coefficient.

C. Threshold Switching Voltage Drift and Temperature Dependence

The temperature dependence of the RESET state drift can also be measured from threshold switching voltage $V_{\rm th}$ drift measurement. The PCM cell on the MTS is programmed into the full RESET state, and $V_{\rm th}$ is read at 25 °C, whereas the cells are annealed at various annealing temperatures T_A before reading $V_{\rm th}$. To read $V_{\rm th}$, a single triangle pulse that ramps up is applied to the RESET state. Once $V_{\rm th}$ is reached, the current through the PCM cell suddenly increases (see Fig. 9). By monitoring the current through the PCM cell, $V_{\rm th}$ can be determined from the ramp rate of the pulse and the time it takes to threshold switch, i.e., $t_{\rm th}$.

To measure the $V_{\rm th}$ drift behavior, $V_{\rm th}$ is read at 100 μs; 1, 10, and 100 ms; and 1 s after RESET programming. $V_{\rm th}$ is read only once per RESET programming since the cells can be partial-SET programmed by $V_{\rm th}$ measurement. The annealing of PCM cells starts 10 μs after RESET programming. The annealing temperature T_A is varied between 25 °C (no annealing) and 185 °C.

Fig. 10(a) shows the $V_{\rm th}$ drift over time with various T_A. It confirms that the drift is faster at higher annealing temperature resulting in higher $V_{\rm th}$. By fitting the data according to (2), the $V_{\rm th}$ drift coefficient can be found as a function of T_A [see Fig. 10(b)]. As we have seen from the $R_{\rm RESET}$ drift measurement, the drift coefficient of $V_{\rm th}$ drift also shows the tendency to increase as temperature increases.

V. Drift Model Comparison

As it has been mentioned in the introduction, various models for the drift mechanism have been proposed in the past years. Those include the models based on the trap decay [7]–[9], generation of the donor/acceptor defect pairs [6], [13], and mechanical stress release [10]. In the previous sections, we derive analytical expressions and interpret our measurement data based on the trap decay model.

Nonetheless, our analysis and results on temperature dependence do not conclude that the trap decay model is the only valid model. With more or less rigorousness, different drift models can lead to the same temperature dependence. The mechanical stress release model [10] also implies the identical temperature dependence for the drift coefficient with constant annealing temperature as the model derivation leads to the following expression for the drift coefficient:

$$\nu=\frac{u_0 D}{\Delta W_B}\frac{T_A}{T_R} \tag{10}$$

where u_0, D, and ΔW_B are the maximum dilation, the deformation potential, and the difference between the maximum and minimum barrier heights, respectively. The donor/acceptor

defect pair model [13] also suggests that the similar temperature dependence can be implemented once the temperature dependence of the defect pair generation rate is included in the model.

The analytical expression for the drift model with time-varying annealing temperature in (7) is derived from the common phenomenological model in (1), which all drift models agree on. The assumption that the same R_{RESET} corresponds to the same RESET state is applicable regardless of how each model defines the RESET state (e.g., trap density, band gap, and donor/acceptor defect pair density). Therefore, the analytical expression for the drift model with time-varying annealing temperature also does not exclude any drift model to be invalid.

VI. Conclusion

In this paper, we have measured the drift coefficients of the RESET resistance R_{RESET} and threshold switching voltage V_{th} in PCM and their temperature dependence in a microsecond time scale using a novel measurement structure, i.e., the MTS. The MTS places a metal heater in close proximity of the PCM programmed region to reduce thermal time constant and accurately control the temperature. Using PCM cells with an MTS, we have extended the temperature-dependent measurement on the R_{RESET} and V_{th} drifts down to 100 μs for the PCM cells constantly annealed at temperatures between 25 °C and 180 °C while maintaining the fixed programming and reading temperature at 25 °C. We have experimentally shown that the existing phenomenological model for the drift is applicable down to a microsecond time scale for a wide range of annealing temperatures. We have found that the measured temperature dependence of the drift coefficient for constant annealing temperature is proportional to the annealing temperature, as expected from the trap decay model with distributed trap energy [7]–[9]. Based on the phenomenological drift model for constant annealing temperature, we have derived an analytical expression that can explain the drift behavior for time-varying annealing temperature and have shown that it agrees well with the experimental results from the MTS. This analytical expression will lead to better assessment of the thermal disturbance effect on the R_{RESET} and V_{th} drifts and the resultant variations in them.

References

[1] G. Servalli, "A 45 nm generation phase change memory technology," in *IEDM Tech. Dig.*, 2009, pp. 113–116.

[2] R. Bez, "Chalcogenide PCM: A memory technology for next decade," in *IEDM Tech. Dig.*, 2009, pp. 89–92.

[3] A. Pirovano, A. L. Lacaita, A. Benvenuti, F. Pellizzer, and R. Bez, "Electronic switching in phase-change memories," *IEEE Trans. Electron Devices*, vol. 51, no. 3, pp. 452–459, Mar. 2004.

[4] V. G. Karpov, Y. A. Kryukov, S. D. Savransky, and I. V. Karpov, "Nucleation switching in phase change memory," *Appl. Phys. Lett.*, vol. 90, no. 12, p. 123 504, Mar. 2007.

[5] D. Ielmini and Y. Zhang, "Analytical model for subthreshold conduction and threshold switching in chalcogenide-based memory devices," *J. Appl. Phys.*, vol. 102, no. 5, p. 054 517, Sep. 2007.

[6] A. Pirovano, A. L. Lacaita, F. Pellizzer, S. A. Kostylev, A. Benvenuti, and R. Bez, "Low-field amorphous state resistance and threshold voltage drift in chalcogenide materials," *IEEE Trans. Electron Devices*, vol. 51, no. 5, pp. 714–719, May 2004.

[7] D. Ielmini, S. Lavizzari, D. Sharma, and A. L. Lacaita, "Physical interpretation, modeling and impact on phase change memory (PCM) reliability of resistance drift due to chalcogenide structural relaxation," in *IEDM Tech. Dig.*, 2007, pp. 939–942.

[8] D. Ielmini, D. Sharma, S. Lavizzari, and A. L. Lacaita, "Reliability impact of chalcogenide-structure relaxation in phase-change memory (PCM) cells—Part I: Experimental study," *IEEE Trans. Electron Devices*, vol. 56, no. 5, pp. 1070–1077, May 2009.

[9] S. Lavizzari, D. Ielmini, D. Sharma, and A. L. Lacaita, "Reliability impact of chalcogenide-structure relaxation in phase-change memory (PCM) cells—Part II: Physics-based modeling," *IEEE Trans. Electron Devices*, vol. 56, no. 5, pp. 1078–1085, May 2009.

[10] I. V. Karpov, M. Mitra, D. Kau, G. Spadini, Y. A. Kryukov, and V. G. Karpov, "Fundamental drift of parameters in chalcogenide phase change memory," *J. Appl. Phys.*, vol. 102, no. 12, p. 124 503, Dec. 2007.

[11] D. Ielmini, A. L. Lacaita, and D. Mantegazza, "Recovery and drift dynamics of resistance and threshold voltages in phase-change memories," *IEEE Trans. Electron Devices*, vol. 54, no. 2, pp. 308–315, Feb. 2007.

[12] S. Raoux, J. L. Jordan-Sweet, and A. J. Kellock, "Crystallization properties of ultrathin phase change films," *J. Appl. Phys.*, vol. 103, no. 11, p. 114 310, Jun. 2008.

[13] A. Redaelli, A. Pirovano, A. Lacatelli, and F. Pellizzer, "Numerical implementation of low field resistance drift for phase change memory simulations," in *Proc. NVSMW/ICMTD*, 2008, pp. 39–42.

[14] D. Ielmini, S. Lavizzari, D. Sharma, and A. L. Lacaita, "Temperature acceleration of structural relaxation in amorphous $Ge_2Sb_2Te_5$," *Appl. Phys. Lett.*, vol. 92, no. 19, p. 193 511, May 2008.

[15] D. Ielmini, M. Boniardi, A. L. Lacaita, A. Redaelli, and A. Pirovano, "Unified mechanisms for structural relaxation and crystallization in phase-change memory devices," *Microelectron. Eng.*, vol. 86, no. 7–9, pp. 1942–1945, Jul.–Sep. 2009.

[16] S. Kim, B. Lee, M. Asheghi, G. A. M. Hurkx, J. Reifenberg, K. Goodson, and H.-S. P. Wong, "Thermal disturbance and its impact on reliability of phase-change memory studied by micro-thermal stage," in *Proc. IEEE IRPS*, Anaheim, CA, May 2–6, 2010, pp. 99–103.

[17] A. Pirovano, A. L. Lacaita, A. Benvenuti, F. Pellizzer, S. Hudgens, and R. Bez, "Scaling analysis of phase-change memory technology," in *IEDM Tech. Dig.*, 2003, pp. 29.6.1–29.6.4.

[18] U. Russo, D. Ielmini, A. Redaelli, and A. L. Lacaita, "Modeling of programming and read performance in phase change memories—Part II: Program disturb and mixed scaling approach," *IEEE Trans. Electron Devices*, vol. 55, no. 2, pp. 515–522, Feb. 2008.

[19] D. Ielmini and Y. Zhang, "Physics-based analytical model of chalcogenide-based memories for array simulation," in *IEDM Tech. Dig.*, 2006, pp. 401–404.

[20] M. Boniardi, A. Redaelli, A. Pirovano, I. Tortorelli, D. Ielmini, and F. Pellizzer, "A physics-based model of electrical conduction decrease with time in amorphous $Ge_2Sb_2Te_5$," *J. Appl. Phys.*, vol. 105, no. 8, p. 084 506, May 2009.

[21] D. Tio Castro, L. Goux, G. A. M. Hurkx, K. Attenborough, R. Delhougne, J. Lisoni, F. J. Jedema, M. A. A. in't Zandt, R. A. M. Wolters, D. J. Gravesteijn, M. A. Verheijen, M. Kaiser, R. G. R. Weemaes, and D. J. Wouters, "Evidence of the thermo-electric Thomson effect and influence on the program conditions and cell optimization in phase-change memory cells," in *IEDM Tech. Dig.*, 2007, pp. 315–318.

[22] R. B. Belser and W. H. Hicklin, "Temperature coefficients of resistance of metallic films in the temperature range 25 ° to 600 °C," *J. Appl. Phys.*, vol. 30, no. 3, pp. 313–322, Mar. 1959.

SangBum Kim received the B.S. degree from Seoul National University, Seoul, Korea, in 2001 and the M.S. and Ph.D. degrees from Stanford University, Stanford, CA, in 2005 and 2010, respectively, all in electrical engineering. His Ph.D. dissertation focused on scalability and reliability of phase-change memory (PCM), including scaling rule analysis, germanium nanowire diode as a scalable selection device, thermal disturbance, drift, and threshold switching.

He has held intern positions at Samsung Advanced Institute of Technology (SAIT) in 2007, working on PCM characterization, and the IBM. T. J. Watson Research Center, Yorktown Heights, NY, in 2007, working on higher k gate dielectrics. He is currently a Postdoctoral Researcher with the IBM T. J. Watson Research Center. His current research interests are characterization and modeling of PCM devices.

Dr. Kim was the recipient of The Korea Foundation for Advanced Studies Scholarship and Samsung Scholarship to support his M.S. and Ph.D. studies, respectively.

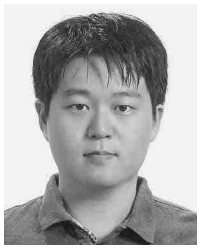

Byoungil Lee received the B.S. degree in electrical engineering from Korea Advanced Institute of Science and Technology, Daejeon, Korea, in 2005 and the M.S. degree in electrical engineering from Stanford University, Stanford, CA, in 2007. He is currently working toward the Ph.D. degree in electrical engineering with Stanford University.

His research interests are on resistive nonvolatile memory devices, including metal–oxide memory and phase-change memory.

Mr. Lee has been a recipient of the Samsung Scholarship since 2005.

Mehdi Asheghi received the Ph.D. and postdoctoral degrees from Stanford University, Stanford, CA, in 1999 and 2000, respectively, conducting research in the area of nanoscale thermal engineering of microelectronic devices.

He is currently a Consulting Associate Professor with Stanford University, focusing on further development of PCRAM technology. He led a well-known and funded research program (2000–2006) at the Carnegie Mellon University, Pittsburgh, PA, which focused on nanoscale thermal phenomena in semiconductor and data storage devices. He is the author of more than 110 book chapters, journal publications, and fully reviewed conference papers.

Fred Hurkx was born in Best, The Netherlands, in 1956. He received the M.Sc. degree in physical engineering and the Ph.D. degree from Technical University of Eindhoven, The Netherlands, in 1985 and 1990, respectively. His thesis involved the modeling of downscaled bipolar transistors.

In 1979, he joined Philips Research Laboratories, Eindhoven, where he has been working in the field of semiconductor research since 1983. He is currently with NXP-TSMC Research Center, Leuven, Belgium.

John P. Reifenberg received the B.S. degree (with Departmental, College, and University Honors) from Carnegie Mellon University, Pittsburgh, PA, in 2003 and the M.S. and Ph.D. degrees from Stanford University, Stanford, CA, in 2006 and 2010, respectively, all in mechanical engineering. His graduate research focused on photothermal and electrical metrology techniques, modeling, and experimental design for understanding nanoscale thermal phenomena in phase-change memory devices.

During his graduate work, he interned at the Intel Corporation, developing phase-change memory device measurement techniques. He is currently a Senior Process Engineer with Intel Corporation, Santa Clara, CA. His responsibilities center on the development of electron-beam lithography systems to advance photomask technology. His interests are in nanoscale thermal physics, nanoscale materials design and metrology, device modeling, design of experiment, and manufacturing optimization.

Dr. Reifenberg was a recipient of the Honorary Stanford Graduate Fellowship. His graduate studies were supported by a National Defense Science and Engineering Graduate Fellowship through the Office of Naval Research.

Kenneth E. Goodson received the Ph.D. degree from the Massachusetts Institute of Technology (MIT), Cambridge, in 1993.

He is currently a Professor and the Vice Chair of Mechanical Engineering with Stanford University, Stanford, CA, where his group studies thermal phenomena in electronic nanostructures and energy conversion devices. His doctoral alumni include Professors at the University of California, Berkeley, MIT, the University of California, Los Angeles, the University of Illinois at Urbana-Champaign, and the University of Michigan, Ann Arbor, as well as staff at Intel, AMD, and IBM. He has coauthored more than 120 archival journal articles, 24 patents, two books, and eight book chapters. He is a founder and former CTO of Cooligy, which builds microcoolers for computers and was acquired in 2005 by Emerson.

Dr. Goodson was the recipient of the Allan Kraus Thermal Management Medal from the American Society of Mechanical Engineers (ASME), the Office of Naval Research (ONR) Young Investigator Award, and the National Science Foundation (NSF) Career Award. He was also the recipient of the Outstanding Reviewer Award from the *ASME Journal of Heat Transfer*, for which he served as an Associate Editor. He was a JSPS Visiting Professor at The Tokyo Institute of Technology and is the Editor-in-Chief of *Nanoscale and Microscale Thermophysical Engineering*. His research has been recognized through keynote lectures at INTERPACK, ITHERM, and Therminic, as well as best paper awards at SEMI-THERM, SRC TECHCON, and the IEDM.

H.-S. Philip Wong received the B.Sc. (Hons.) degree from The University of Hong Kong, Pokfulam, Hong Kong, in 1982, the M.S. degree from the State University of New York, Stony Brook, in 1983, and the Ph.D. degree from Lehigh University, Bethlehem, PA, in 1988, all in electrical engineering.

He joined the IBM T. J. Watson Research Center, Yorktown Heights, New York, in 1988. While at IBM, he worked on CCD and CMOS image sensors, double-gate/multigate MOSFETs, device simulations for advanced/novel MOSFETs, strained silicon, wafer bonding, ultrathin-body SOIs, extremely short gate FETs, germanium MOSFETs, carbon nanotube FETs, and phase-change memory. He held various positions from Research Staff Member to Manager, and Senior Manager. While he was Senior Manager, he had the responsibility of shaping and executing IBM's strategy on nanoscale science and technology, as well as exploratory silicon devices and semiconductor technology. In September 2004, he joined Stanford University, Stanford, CA, as a Professor of electrical engineering. His research interests are in nanoscale science and technology, semiconductor technology, solid-state devices, and electronic imaging. He is interested in exploring new materials, novel fabrication techniques, and novel device concepts for future nanoelectronics systems. Novel devices often enable new concepts in circuit and system designs. His research also includes explorations into circuits and systems that are device driven. His present research covers a broad range of topics, including carbon nanotubes, semiconductor nanowires, self-assembly, exploratory logic devices, nanoelectromechanical devices, novel memory devices, and biosensors.

Prof. Wong served on the IEEE Electron Devices Society as an Elected Administrative Committee Member from 2001 to 2006. He served on the IEEE International Electron Devices Meeting Committee from 1998 to 2007 and was the Technical Program Chair in 2006 and the General Chair in 2007. He served on the IEEE International Solid- State Circuits Conference Program Committee from 1998 to 2004 and was the Chair of the Image Sensors, Displays, and MEMS Subcommittee from 2003 to 2004. He serves on the Executive Committee of the Symposia of VLSI Technology and Circuits. He was the Editor-in-Chief of the IEEE TRANSACTIONS ON NANOTECHNOLOGY in 2005–2006. He has been a Distinguished Lecturer of the IEEE Electron Devices Society since 1999 and was a Distinguished Lecturer of the Solid-State Circuit Society from 2005 to 2007.